16th World Conference on Earthquake Engineering, 16WCEE 2017
Santiago Chile, January 9th to 13th 2017
Paper N° 4571
Registration Code: S-V1464760664

DETAILED NONLINEAR MODELING, PUSHOVER AND TIME HISTORY ANALYSIS OF ALTO RIO BUILDING USING BEAM-TRUSS MODEL

P. Zhang[1], J.P. Conte[2], J.I. Restrepo[3], J. Ou[4]

[1] Ph.D. candidate, Dalian University of Technology, Faculty of Infrastructure Engineering, zpz_87@163.com
[2] Professor, University of California, San Diego, Department of Structural Engineering, jpconte@ucsd.edu
[3] Professor, University of California, San Diego, Department of Structural Engineering, jrestrepo@ucsd.edu
[4] Professor, Dalian University of Technology, Faculty of Infrastructure Engineering, oujinping@dlut.edu.cn

Abstract

The fifteen-story Alto Rio building built in 2006 in the city of Concepción, Chile, was the only modern building that collapsed catastrophically during the February 27, 2010 Mw 8.8 Maule earthquake, resulting in eight human casualties. This building was typical of many medium rise reinforced concrete bearing wall buildings designed and built in Chile during the period 1996-2009. Understanding the response behavior and collapse mechanism of the Alto Rio building during the Maule earthquake is very important for the earthquake engineering community. For this purpose, a detailed three-dimensional nonlinear model of the complete Alto Rio building was developed in the OpenSees analysis framework using the beam-truss modeling approach. The geometry of the structure was obtained directly from the AutoCAD design documents of Alto Rio. Realistic cyclic material constitutive models were used for the reinforcing steel and concrete materials. This paper discusses some details of the building model and key results obtained from a nonlinear pushover analyses and a nonlinear time history analysis, which shed some light on the cause of collapse of the Alto Rio building.

Keywords: Bearing wall building, Maule earthquake, collapse, beam-truss model, nonlinear time history analysis

1. Introduction

The M_w 8.8 Maule earthquake that occurred in the coastal region of central Chile on February 27, 2010 had significant impact on the lives of over 8 million people. This earthquake resulted in five hundred and twenty five casualties [1], and direct economic losses assessed at 20 billion dollars, corresponding to 9% of Chile's gross domestic product [2]. During this earthquake, a significant percentage of modern reinforced concrete (RC) bearing wall buildings exhibited moderate to severe structural damage [1]. One building, the 15-story Alto Rio building, located in the city of Concepcion, experienced catastrophic collapse in its transverse direction, see Fig. 1, which resulted in the loss of eight lives. IDIEM [3, 4] and DICTUC [5] report a detailed forensic field investigation, which includes a description and photographic evidence of the extent of damage in inaccessible areas of the building. Various researchers have made use of the forensic data available and have tested a number of hypotheses. Alimoradi and Naeim [6] investigated whether the large (3.0 m) westward co-seismic displacement played a major role in the collapse of the Alto Rio building. Song et al.[7] analyzed the collapse of the building from mainly a qualitative point of view based on field observations and identified several local failures that could have contributed to the collapse of this building. Kohrangi et al. [8] performed an assessment of the building according to FEMA 356 [9] and determined that this prestandard revealed a few weaknesses in the building. Deger and Wallace [10] developed a model of a slice of Alto Rio and showed that the seismic response of this slice was sensitive to the detailing of the walls' boundary elements. A similar slice was analyzed by Willford [11] using nonlinear shell elements to reveal problems with the detailing of boundary elements in the walls. The only investigation carried out at the system level is that reported by Restrepo et al. [12]. These researchers modeled the entire Alto Rio building with nonlinear shell elements and performed parametric static pushover analyses. They found that the collapse of the Alto Rio building was most likely triggered by the compressive failure of the curved walls surrounding the staircase. This paper builds on the work of Restrepo et al. and discusses the development of a detailed nonlinear three-dimensional (3D) finite element (FE) model of the entire Alto Rio building in the open source software framework OpenSees [13]. The development of the model and key results of the pushover and time-history analyses are described in the following sections.

(a)  (b) 

Fig. 1 – Alto Rio building located in Concepcion, Chile: (a) before the earthquake[14]; (b) after the earthquake[15]

2. Description of the building

2.1 Structural design

Alto Rio was a fifteen story mixed-use building with a tower and two underground parking levels, see Fig. 1. This building was built in the city of Conception, Chile at coordinates 36.828°S and 73.062°W and its longitudinal axis was oriented N26.67°W, see Fig. 2. Construction of the Alto Rio building took place between December 2007 and February 2009. The Alto Rio building had a 0.8 m thick RC mat foundation below the tower and 0.4 m thick foundation to support the underground parking levels to the side of the tower. The underground parking levels were enclosed by 250 mm thick RC retaining walls. The staircase was enclosed by walls on gridlines 26 and 34 that had a curved corner at gridline J, see Fig. 2. Other detailed geometric information is provided in [12].

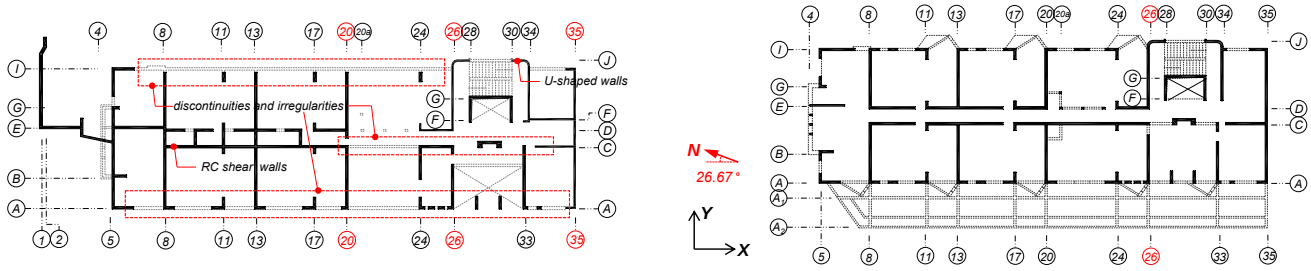

Fig. 2 – Structural plans: (a) first floor level (Level F0); (b) second floor level (Level F1)

The Alto Rio building was designed in accordance with the Chilean RC building code NCh 430-96 [16], which was developed based on the provisions of the *Building Code Requirements for Reinforced Concrete*, ACI 318-05 [17, 18] with one notable exception: NCh430 does not contain prescriptive requirements for boundary elements in RC walls. The walls in this building contained longitudinal reinforcement at the wall ends and intersections consisting of 2Φ16mm (4Φ16mm) or 2Φ22mm (4Φ22mm) bars, and with minimum or near minimum longitudinal and transverse reinforcement elsewhere. As discussed by Restrepo et al. [1], the transverse reinforcement in the curved walls around the staircase is deficient since the concrete cover on the concave side of the wall has to resist the radial forces developing when the horizontal reinforcement in this side of the wall is subjected to tension. The building also contained a number of irregularities in the first story (above ground). Such irregularities consisted of changes in the cross-section geometry of a number of walls and gravity columns. For example, the walls along gridline I were discontinued at Level F1, and the length of the walls along gridlines 8, 13 and 20 was reduced from 5.0 m to 4.6 m. These transverse walls had no flange on the east side (along axis I) at Level F0, but had a flange at Levels F1 and above. The wall along gridline J between axes 26 and 28 contained a doorway just below Level F0, which resulted in some stress concentration.

2.2 Material characterization

2.2.1 Concrete

Design concrete cylinder compressive strengths of 20 MPa (HB25) and 25 MPa (H30) at 28 days were specified above and below the second floor, respectively. In order to determine the actual properties of the concrete of the building, fifty-one cores were extracted from walls in the collapsed building [3]. The results of the tests were divided into two groups, see Table 1. Group I characterizes the concrete in the basement and at Levels 1 and 2, while Group II characterizes the concrete at Level 3 and above.

Table 1 – Design and measured concrete compressive strengths

Concrete	**Design concrete compressive strength**		**Measured concrete compressive strength**		
	Concrete type	$f_c^{'}$ [MPa]	$f_c^{'}$ [MPa]	Standard deviation [MPa]	Specific density
Group I	HB30	25.0	42.4	6.4	2.36
Group II	HB25	20.0	48.8	7.1	2.36

Note: $f_c^{'}$ = 42.4 MPa and E_c = 30.8 GPa were used for the whole building in the following FE analysis.

2.2.2 Reinforcing steel

The building incorporated 8 mm and 10 mm bars as wall web reinforcement, 8, 10 and 12 mm bars as slab reinforcement, and 16, 18 and 22 mm bars for the wall boundary longitudinal reinforcement. Typical horizontal and vertical wall web reinforcement consisted of 8 mm bars spaced at 150 mm to 200 mm (10 mm bars were used in some transverse walls). All reinforcement was specified as S420, which has a specified yield strength of 420 MPa. IDIEM [3] and DICTUC [5] report the mechanical properties for 85 bars extracted from the collapsed building. It was found that 20 of the bars sampled had yielded. A study of the bar properties of the 65 bars that had not shown signs of yielding indicates that the mechanical properties depended on the bar size. This prompted the need to classify the bars in two different types, each with distinct mechanical properties, see Table 2.

Table 2 – Average mechanical properties of the reinforcing steel extracted from the Alto Rio Building

Types	**Diameters [mm]**	**No. samples**	f_y **[MPa]**	f_{su} **[MPa]**	E_s **[GPa]**	ε_{su}
Type I (S420)	8, 10, 12	16	509.0	746.0	200.0	0.12
Type II (S420)	16, 18, 22, 25	49	472.0	727.0	200.0	0.12

2.3 Ground motion recording

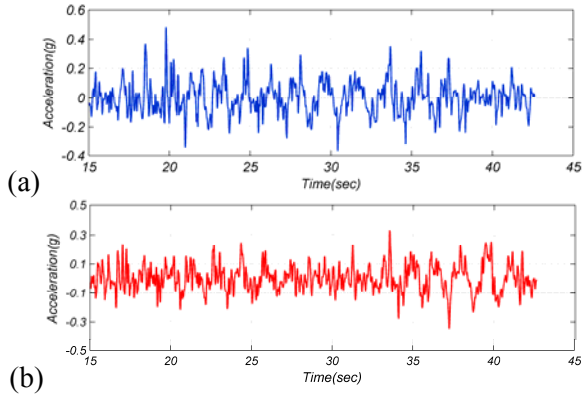

Fig. 3 – Blended horizontal ground motion components in Concepcion: (a) S63°W; (b) N27°W

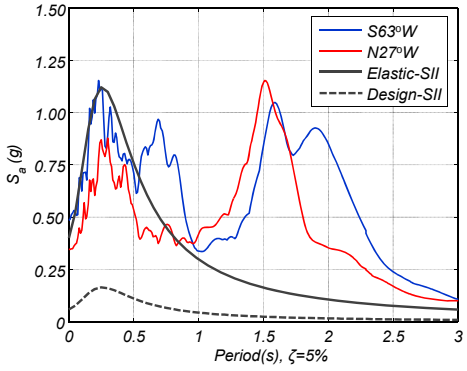

Fig. 4 – Linear elastic pseudo-acceleration response spectra of the ground motion records

During the Maule earthquake, the ground motion was recorded by an analog-film accelerograph station CONC located at the Inmaculada Concepción School (36.828°S, 73.048°W) and by a digital GPS station CONZ

(36.844°S, 73.026°W) [19-21] both in close proximity of the Alto Rio building. The accelerograph station CONC captures well the high-frequency ground motion components and resonance effects of the basin, whereas the GPS station CONZ captures well the low-frequency components of the basin motion at 1 s sampling rate. The ground motion time histories recorded at CONC and CONZ were blended in order to obtain broadband three-dimensional components of the ground motion used in the analysis presented in this paper. Fig. 3 shows the acceleration time histories between t = 15.0 s and 42.5 s of the blended horizontal ground motion components. Note that the horizontal ground motion components were rotated and aligned with the longitudinal (N27°W) and transversal (S63°W) axes of the Alto Rio building. The S63°W and N27°W components of the ground displacement clearly show the resonance period of the Concepcion basin at about 2 s reported by others [22, 23]. Fig. 4 depicts the 5% damped elastic pseudo-acceleration response spectra of the two horizontal ground motion components. It also shows the elastic response spectrum (5% damping) and design spectrum for soil type II in seismic zone III as determined from the Chilean code for seismic design of buildings NCh433 [16].

3. Nonlinear finite element model

3.1 Modeling approach and finite element models used

To better understand the causes of collapse of the Alto Rio building, a detailed nonlinear 3D FE model of the building was created using the beam-truss modeling (BTM) approach [24], which was developed based on the nonlinear cyclic truss model [25]. The BTM approach, see Fig. 5, to model and simulate the nonlinear response behavior of RC walls and slabs was validated extensively through experimental-analytical correlation studies [24, 26]. According to the BTM approach, RC walls are modeled using nonlinear Euler-Bernoulli fiber-section beam-column elements to represent the concrete and reinforcing steel in the longitudinal (vertical) direction of the wall, and nonlinear truss elements to represent (for the in-plane behavior of the wall) the reinforcing steel and concrete in the transverse direction of the wall and the concrete in the diagonal directions of the wall. Furthermore, elastic beams with zero axial stiffness parallel to the transverse truss elements are used to represent the out-of-plane behavior of the wall, see Fig. 5. In modeling slabs, the main difference with walls is that nonlinear fiber-section beam-column elements are used in both directions of the slab to capture both the in-plane and out-of-plane behavior. The diagonal nonlinear truss elements are assigned a bi-axial material model for concrete that accounts for the effect of the normal tensile strain on the stress-strain behavior of concrete in compression [27] and compensates for mesh-size effects (ensures mesh objectivity) as proposed by Lu and Panagiotou [24]. Other details about the BTM approach are presented in [24, 26]. The type and composition of the elements used in the BTM of the Alto Rio building as well as the material constitutive models assigned to them play an important role in the 3D prediction of the response (global and local aspects) of Alto Rio to the 2010 Maule earthquake. The materials constitutive models used in this study are briefly presented in the next section.

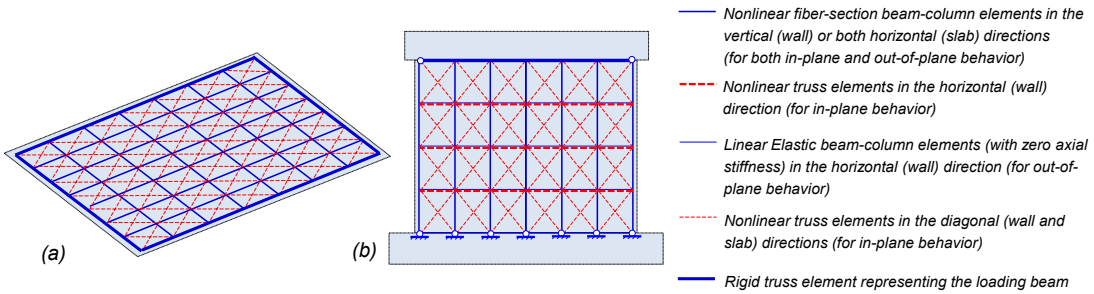

Fig. 5 – Schematic description of the beam-truss modeling approach for (a) RC slabs and (b) RC shear walls

3.2 Constitutive material models

(1) Concrete. In this study, the modified Kent-Park-Scott model [28], referred to as Concrete02 in OpenSees, was used to simulate the behavior of the unconfined concrete in all vertical and horizontal elements of all walls and slabs. The uniaxial material model developed by Lu and Panagiotou [24], referred to as ConcretewBeta in OpenSees, was used to simulate the unconfined concrete in all diagonal truss elements of all walls and slabs. This material model accounts for the instantaneous effect of the transverse tensile strain on the compressive

strength according to experimental observations by Vecchio and Collins [27] and the ensuing modified compression field theory. Thus, at every step of a nonlinear analysis, the compressive stresses of the diagonal truss elements are multiplied by a reduction coefficient, β, which expresses the adverse effect of transverse tension on the compressive stress-strain behavior of concrete. Therefore, every diagonal truss element requires the definition of an additional pair of nodes to establish a fictitious 'strain gauge' element that allows the calculation of the transverse strain, ε_n, as explained in detail in [24]. In this study, a zero tensile strength was used for all diagonal truss elements. The backbone curve parameters for unconfined concrete behavior in both models (Concrete02 and ConcretewBeta) were defined based on the measured material properties presented in Section 2.2 and reported in Table 1. Based on the steel reinforcement details in the Alto Rio building, it was assessed that all concrete could be considered as unconfined. To ensure the objective prediction of the localization of inelastic deformations, the strength degrading branches of the two concrete models (Concrete02 and ConcretewBeta) were scaled based on the length of the element and the fracture energy of concrete [24, 26, 29].

(2) Reinforcing steel. The well-known Giuffre–Menegotto–Pinto (GMP) material model [30], referred to as Steel02 in OpenSees, was used to simulate the behavior of the reinforcing steel in the model of Alto Rio. This model captures well the Bauschinger effect and the cyclic hysteretic behavior of reinforcing steel [30]. A detailed description of the model and its parameters is provided in [30]. The parameter values of the GMP models used for Type I and Type II steel, respectively, were determined based on the material tests results presented in Section 2.2 and reported in Table 2. In addition, parameters R_0 = 18.5, cR_1 = 0.925, and cR_2 = 0.15 with isotropic strain hardening in compression only were applied for the transition curve between the elastic and plastic branches [30] for Type I and Type II steel. It is important to mention that the GMP model used in this study does not capture the effects of bar buckling, bond-slip, bar facture, anchorage loss (lap-splices), and low-cycle fatigue (followed by bar fracture) on the behavior of the reinforcing steel.

3.3 Matlab-based pre and post-processor

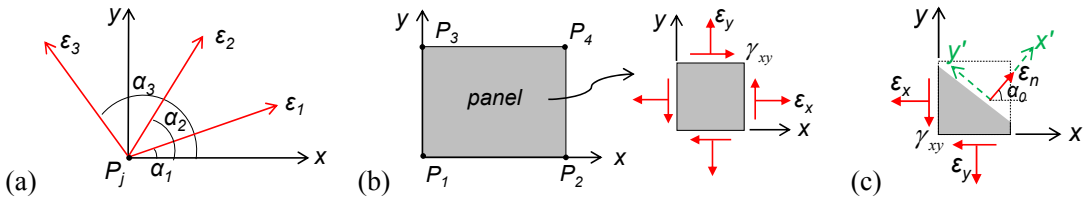

Fig. 6 – Method to calculate principal strains and maximum shear strain in a panel: (a) description of three measured strains in the panel local coordinate system; (b) equivalent strain state in a panel; (c) equivalent principal strain state according to Mohr's circle for plane strain condition

In support of the study presented in this paper, a pre- and post-processor tool was developed in the Matlab programming environment [31] to build detailed 3D FE models of large-scale structures (such as the Alto Rio building) using the BTM approach or shell elements in OpenSees. It was designed to support the common needs in modeling and analyzing 2D and 3D RC shear wall building structures, from pre- to post-processing, including geometric modeling, automated FE meshing, definition of analyses to be performed, OpenSees model generation, and visualization of analytical results. Post-processing Matlab functions were developed to support several widely used types of visualization of the analytical results. A software interface was also developed to make use of GiD, a powerful pre- and post-processor for numerical simulations in science and engineering [32], to visualize the structural response simulation results obtained from OpenSees. Furthermore, a post-processing tool was developed to compute the equivalent principal strains and maximum shear strain in every single wall or slab panel according to Mohr's circle for plane strain transformation, and to generate color-coded contour plots of these strain quantities. According to Mohr's circle for plane strain transformation, three recorded axial strains ε_i (i = 1, 2, 3) at angles α_i (i = 1, 2, 3) at point P_j (j = 1, 2, 3, 4), see Fig. 6(a), can be represented by the axial strains ε_{x,P_j}, ε_{y,P_j} and shear strain γ_{xy,P_j} as shown in Eq. (2). These equations are solved for the strains ε_{x,P_j}, ε_{y,P_j}, and γ_{xy,P_j} at point P_j (j = 1, 2, 3, 4) from which the principal strain components $\varepsilon_{\max,P_j}$ and $\varepsilon_{\min,P_j}$, and maximum

shear strain (shear angle) $\gamma_{\max,P_j}$ at point P_j are calculated from Eq. (3). Then the equivalent principal strains $\varepsilon_{\max}$ and $\varepsilon_{\min}$, and maximum shear strain $\gamma_{\max}$ are obtained from Eq. (4) and illustrated in Fig. 6(c).

$$\varepsilon_{i,P_j} = \frac{\varepsilon_{x,P_j} + \varepsilon_{y,P_j}}{2} + \frac{\varepsilon_{x,P_j} - \varepsilon_{y,P_j}}{2}\cos 2\alpha_i - \frac{\gamma_{xy,P_j}}{2}\sin 2\alpha_i \quad (i = 1, 2, 3;\ j = 1, 2, 3, 4) \tag{2}$$

$$\begin{Bmatrix} \varepsilon_{\max,P_j} \\ \varepsilon_{\min,P_j} \end{Bmatrix} = \frac{\varepsilon_{x,P_j} + \varepsilon_{y,P_j}}{2} \pm \sqrt{\left(\frac{\varepsilon_{x,P_j} - \varepsilon_{y,P_j}}{2}\right)^2 + \left(\frac{\gamma_{xy,P_j}}{2}\right)^2}, \quad \gamma_{\max,P_j} = 2\times\sqrt{\left(\frac{\varepsilon_{x,P_j} - \varepsilon_{y,P_j}}{2}\right)^2 + \left(\frac{\gamma_{xy,P_j}}{2}\right)^2} \tag{3}$$

$$\varepsilon_{\max} = \frac{1}{4}\sum_{j=1}^{4}\varepsilon_{\max,P_j}, \quad \varepsilon_{\min} = \frac{1}{4}\sum_{j=1}^{4}\varepsilon_{\min,P_j}, \quad \gamma_{\max} = \frac{1}{4}\sum_{j=1}^{4}\gamma_{\max,P_j} \tag{4}$$

3.4 Finite element model of Alto Rio building

For the sake of computational efficiency, a detailed 3D FE model of the 15-story Alto Rio building with two underground levels was built in OpenSeesMP [13], the parallel version of OpenSees designed to take advantage of parallel computing for both element state determination and equation solving. Based on the IDIEM report and the final collapse mode pictured in Fig. 1(b), it can be drawn that no evidence existed to suggest that soil-structure interaction played a significant role in the collapse of Alto Rio, and there was also not enough evidence to justify partially restraining (with springs) the lateral degrees of freedoms (DOFs) at the perimeter of the underground levels. Therefore, fixed-based condition was assumed at Level B2 and no lateral support was applied at Levels B1 and F0 as shown in Fig. 7(a). All analyses in this study were performed on a Dell WorkStation (Precision T7610) with two Intel® Xeon® Processor E5-2630 v2 (15M Cache, 2.60 GHz, 6-core processor) using OpenSeesMP with 18 processors on Windows 7.0. General information about the FE model is provided in Table 3.

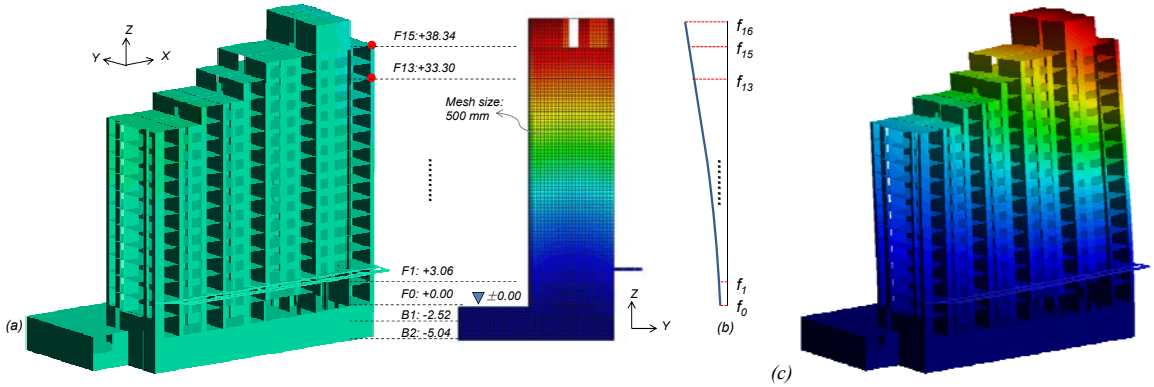

Fig. 7 – Description of FE model: (a) 3D detailed model and profile of south elevation; (b) lateral load pattern used for static pushover analysis; and (c) first mode shape, T_1 = 0.46sec

Table 3 – Basic parameters of Alto Rio FE model

FE model	Mesh size	Nodes	Elements	DOFs	Sections	Materials
Alto Rio	~ 500 mm	59,427	281,440	356,562	1,184	645

4. Analytical results

4.1 Eigen Analysis

Gravity loads consisting of dead and live loads and corresponding inertia (mass) properties (three-directional lumped translational nodal masses) were applied to the structural model of Alto Rio. The dead loads comprised the self-weight of the structure (approximately 1 ton/m^2 of floor) and additional dead loads (ceilings, mechanical

equipment, tiles, kitchen appliances, etc.). For the live loads, 1.96 kN/m^2 (200kgf/m^2) and 4.90 kN/m^2 (500kgf/m^2) were the design loads for the top story and other stories, respectively; as specified by the Chilean code, 25% of these design live loads were assumed to be present during the earthquake and they were further reduced to account for the 70% occupancy rate of Alto Rio at the time of the earthquake. It is noted that the building mass was distributed to the floor FE nodes only. Table 4 reports the total floor masses of the developed FE model of Alto Rio. A vibration eigen analysis of the building was performed based on the tangent stiffness matrix of the FE model after application of the gravity loads. The first mode with a period T_1 of 0.46 sec is predominantly transversal with some torsion as shown in Fig. 7(c). The second mode has a period T_2 of 0.38 sec and is torsional with a center of torsion located between gridlines 24 and 26 (see Fig. 2). The third mode with a period T_3 of 0.33 sec is predominantly longitudinal with some torsion. Based on these eigen analysis results, it is evident that the first mode shape was the dominant deformation pattern of Alto Rio. Therefore, its eigenvector was selected as the load pattern for the static pushover analysis presented next, with the exception that no lateral loads were applied at the two underground levels, see Fig. 7(b).

Table 4 – Mass at each floor of the FE model of Alto Rio

Floors	**B1**	**F0**	**F1**	**F2**	**F3**	**F4**	**F5**	**F6**	**F7**	**F8**	**F9**	**F10**	**F11**	**F12**	**F13**	**F14**	**F15**
M [ton]	894	468	527	439	439	439	439	439	439	439	440	440	426	341	267	214	127

4.2 Static pushover analysis

The 3D nonlinear model of Alto Rio was subjected to gravity analysis, followed by static pushover analysis in the + Y direction using a lateral load pattern associated with the first transversal mode, as described in Fig. 7(b). The nodal pushover forces were only applied to the floor nodes from Level F0 to Level F16 and their spatial distribution followed that of the nodal components in the + Y direction of the first mode shape. In order to achieve good convergence of the static pushover analysis results as the level of nonlinearity increases, the static load control integrator was applied at the early stage of the analysis and then switched at the later stage of the analysis to the static displacement control integrator with a step size of 2.0 mm for the controlled displacement component consisting of the transversal displacement of the control node located at Level F15, see Fig. 7(a). This incremental-iterative pushover analysis consumed 5.1 hours of computational time and stopped converging at a lateral displacement of about 250 mm. The base shear force, base overturning moment and base torque at the ground level (Level F0) are plotted in Fig. 8(a) as a function of the transverse displacement at Level F13 along gridline 35. These are the pushover (capacity) curves of the analysis. The strength demand of the Chilean seismic code for Alto Rio, namely 1.4 times the required overturning moment (M_v) for soil type II [33], is indicated in Fig. 8(a); comparison with the pushover curve for the overturning moment shows that the Alto Rio building had a large reserve of strength and could reliably resist the design forces for soil type II. Three possible reasons for this significant overstrength are given next. Firstly, the measured strength of concrete (about 42.4 MPa) was almost twice higher than the specified strength of 23.0 MPa. Secondly, participation of the wings of the T- or L-shaped walls contributed significantly to the lateral resisting strength of Alto Rio, but these walls were designed as rectangular according to the Chilean seismic code. Thirdly, the contribution of the coupling effect between walls and slabs along the corridor to the lateral strength of the building was often neglected during design, but had considerable impact on the behavior of the building. However, the additional strength contributed by the last two sources might lead to non-ductile (brittle) failure and reduce the structural ductility. The results in Fig. 8(a) show that the building experienced at the load step P_0, corresponding to a roof drift ratio (= ratio of roof transverse displacement at Level F13, 215 mm, over height of F13 above Level B2, i.e., 38.04 m) of 0.56%, an abrupt change in stiffness and significant loss in lateral strength in the + Y direction after reaching a maximum overturning moment of 585.0 MN·m, a maximum base shear of 21.9 MN and a maximum base torque of 531.2 MN·m. Fig. 8(b) presents the maximum inter-story drift ratios and the transverse displacement profile along the height of the building along gridline 35. The lateral stiffness changed drastically at the first and second stories (from Level F0 to Level F2), and the inter-story drift reached the maximum value of 0.79% at the second story (between F1 and F2). Based on the structural design details and analytical results presented here, it is likely that the vertical wall discontinuities and irregularities at the east façade of Alto Rio played a significant role in the initiation and development of the pushover failure mechanism.

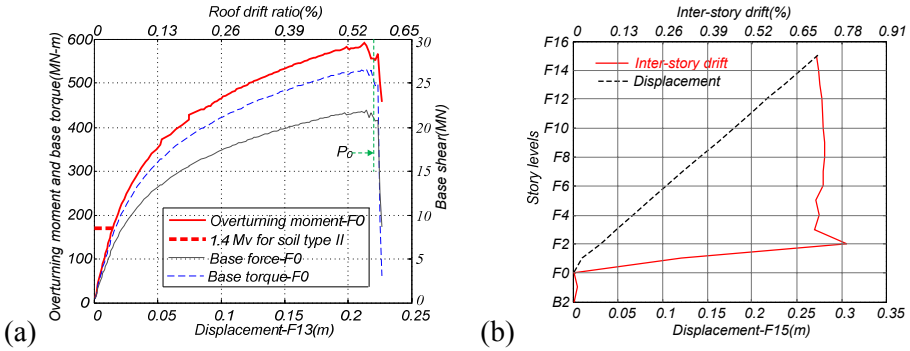

Fig. 8 – Results of static pushover analysis: (a) pushover curves for overturning moment, base shear force and base torque; (b) maximum inter-story drift ratio and displacement profile along the height of the building

To better understand the building behavior at the later stage of the static pushover analysis, the local performance and response of shear walls were examined at load step P_0 (see Fig. 8a). Here, results are presented for the walls along gridline 26. These walls contained most of the features that were considered important when evaluating the possible causes that triggered the collapse of Alto Rio, such as U- and L-shaped walls, openings in walls, wall-slab coupling effect and vertical irregularities. The contour plots of the maximum equivalent principal strain (principal tensile strain) ε_{max}, minimum equivalent principal strain (principal compressive strain) ε_{min} and máximum shear strain γ_{max} obtained using the pre- and post-processor presented in Section 3.3 are shown in Fig. 9 for the walls along gridline 26 at the first two stories (from Level F0 to Level F2) at load step P_0. According to these contour plots, the model predicts significant diagonal cracking in the first two stories of these walls. Fig. 9(a) indicates that the maximum value of ε_{max} is approximately 0.007 on the gridline 26 walls, while Fig. 9(b) shows that the minimum value of ε_{min} is -0.0017 at the bottom of the first story. Other walls presented similar or higher level of damage. For example, the flange of the curved-shaped walls around the staircase at the first story (on gridline J between gridlines 26 and 34) reached the crushing strain of the concrete (about -0.0087). It is important to note that compression failures of concrete walls are extremely fragile and may have caused a redistribution of the gravity loads among the walls of Alto Rio. On Fig. 9(c), the maximum value of the maximum shear strain γ_{max} is 0.0076, indicating significant shear damage in these walls. The pushover analysis results indicate that yielding of the longitudinal reinforcement, crushing of the concrete and relatively large shear strains in a number of transverse walls and in the flanges of walls on gridlines I and J are likely the main reason for the abrupt stiffness and strength losses starting at load step P_0. Large axial and shear strains are concentrated in the walls near the staircase, where the combined actions of the axial, lateral and torsional demands at Level F0 are the greatest during the (first mode) pushover analysis of the Alto Rio building.

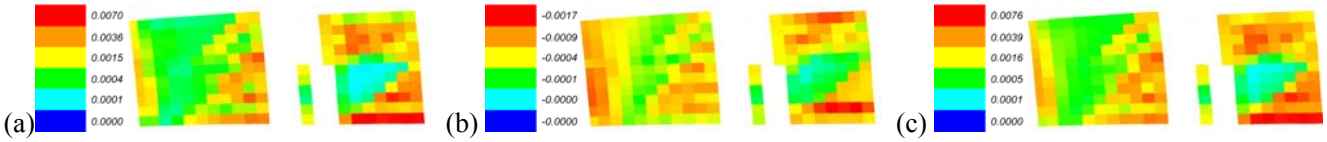

Fig. 9 – Contour plots of equivalent principal tensile and compressive strains and maximum shear strain of the walls along gridline 26 at the first two stories (F0-F2) at load step P_0: (a) ε_{max}, (b) ε_{min}, and (c) γ_{max}

4.3 Time-history analysis

In this section, the 3D nonlinear model of Alto Rio is subjected to the corrected bi-axial horizontal ground motion recorded at the Inmaculada Concepcion station, see Fig. 3. Since the energy dissipation through inelastic material behavior is modeled explicitly in the FE model of Alto Rio, a significantly reduced linear viscous damping ratio of 0.5% was adopted for the Rayleigh damping model used to represent the other sources of energy dissipation [34] for the nonlinear time-history analysis. This damping ratio of 0.5% was applied to the first and third modes and the corresponding mass and stiffness coefficients are α_m = 7.93e-2 /sec and β_k = 3.07e-4 sec, respectively. The cyclic degradation of the material behavior (i.e., progressive stiffness and strength degradation, see Section 3.2) is incorporated in the analysis. Completion of the time history analysis with an integration time

step of 0.005 sec required 61.0 hours using OpenSeesMP with parallel computing. Fig. 10 shows the time-history of the building displacement at Level F15 and gridline 35 in both directions. The building reaches a maximum displacement of 279.6 mm in the +Y direction (241.3 mm at Level F13) at 23.26 sec (denoted as time step P_1 in Fig. 11) and a maximum displacement of 261.4 mm in the -Y direction at 22.78 sec. Based on the pushover analysis presented above and the actual direction of collapse of Alto Rio, the state of the building is examined at its maximum response in the +Y direction. The hysteretic curves of the base shear force and base overturning moment versus the displacement at level F13 superimposed with the corresponding static pushover curves are shown in Fig. 11. It is observed that in the predicted dynamic response to the Maule earthquake, Alto Rio reaches a peak displacement (241 mm) in the +Y direction, which is 12 percent greater than the one reached during the pushover analysis (215 mm) when the computations cease to converge. Given the state of heavy damage (in compression and shear) experienced by the model of Alto Rio under pushover analysis, this suggests that the Alto Rio model is in a state of similar or worse damage when subjected to the Maule earthquake. It is worth noting that it is easier to achieve convergence in nonlinear dynamic analysis than in nonlinear static analysis. The pushover curves for the base shear force and overturning moment shown in Fig. 11 indicate that the building is stronger and more ductile in the -Y than in the +Y direction. The nonlinear pushover and time history analysis results are consistent with each other. It is important to note that the spatial distribution of the equivalent static lateral loads for the dynamic analysis vary at each instant of time and differ from the load pattern assumed for the pushover analysis.

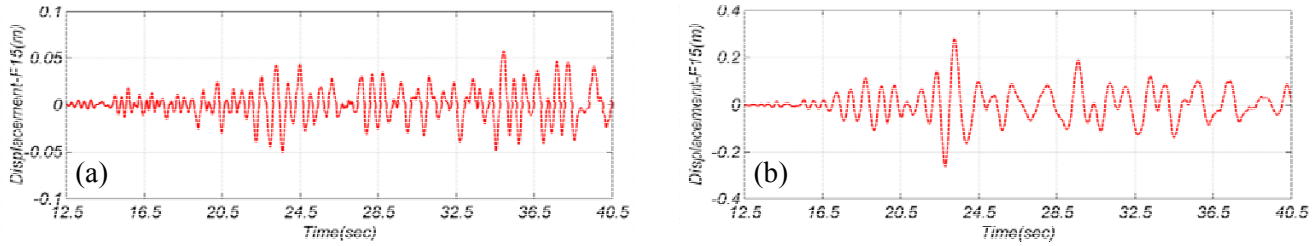

Fig. 10 – Time-history of building displacement at Level F15: (a) X direction, and (b) Y direction

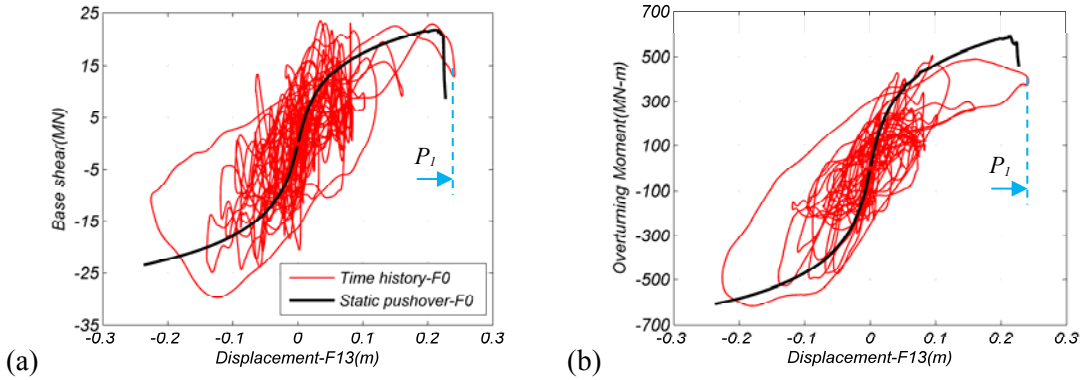

Fig. 11 – Time-history and static pushover analysis results: (a) base shear force – displacement (at F13) hysteretic response; (b) base overturning moment – displacement (at F13) hysteretic response

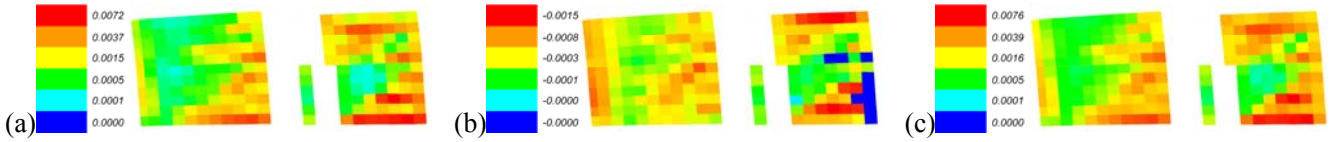

Fig. 12 – Contour plots of principal strains and maximum shear strain for the first two stories (F0-F2) of the walls along gridline 26 at time step P_1: (a) ε_{max}, (b) ε_{min}, and (c) γ_{max}

For consistency with the pushover analysis results discussed in Section 4.2, the local response results obtained for the walls along gridline 26 are presented next. Fig. 12 provides for the first two stories (F0-F2) of these walls the contour plots of the principal (tensile and compressive) strains and the maximum shear strain

obtained at time step P_1 of the nonlinear time history analysis. It is observed that these results are similar to those obtained from the pushover analysis at load step P_0, see Fig. 9.

The pushover and nonlinear time history analyses capture very well the unintended (during design) wall-to-slab coupling along the central corridor running in the longitudinal direction of the building along gridlines C and D. Fig. 13(a) shows the contour plot of the maximum principal strain for the floor slab at Level F12 and at time step P_1. The maximum principal strain recorded in the analysis is 0.003 which is slightly above the yield strain of steel. Yield lines were observed in a similar RC bearing wall building in Chile as a result of the Maule earthquake, see Fig. 13(b). Unintended (during design) wall-to-slab coupling increases the overstrength of a building, but also increases the shear demands on the walls [35].

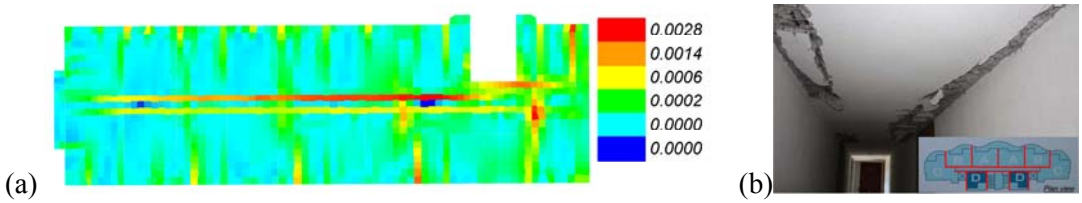

Fig. 13 – Effect of slab-wall coupling: (a) contour plot of maximum principal strain for the floor slab F12 at time step P_1; (b) damage at the slab-wall connections observed in a similar RC building (Courtesy of Dr. P. Dechent)

5. Conclusions

The M_w 8.8 Chile earthquake of February 27, 2010 provided an excellent opportunity to examine the seismic performance of tall RC shear wall buildings. The objective of this paper was to investigate the potential reasons that led to the catastrophic collapse of the Alto Rio building, during which eight people lost their lives. A global detailed three dimensional nonlinear structural model was built in the structural analysis software framework OpenSees using the beam-truss modeling approach. Both a nonlinear static pushover analysis (in the direction of collapse of Alto Rio) and a nonlinear time history analysis were performed to shed some light on the various factors that likely played a role in the collapse of the Alto Rio building. The results obtained from these two types of analysis were close both at the global and local levels, such as for the lateral total base shear demand and strength, total base overturning moment demand and strength, contours of principal (tensile and compressive) strains and maximum shear strains for the walls, and the damage/failure modes of the transverse walls. The Alto Rio building had a large reserve of strength (against lateral loads) due to three main reasons: (i) the measured material strengths are higher than the specified strengths, (ii) the contributions of the wings of the T- and L-shaped walls, which are typically neglected during design, and (iii) the coupling actions between the floor slabs and the walls along the central corridor, which are also typically neglected during design. The additional resistance provided by (ii) and (iii) may lead to non-ductile (brittle) failures and reduce the structural ductility. The analysis results indicate that the configuration and detailing of the reinforcement in this building limited the lateral displacement capacity to relatively small values.

The analysis results obtained in this study point to four potential factors that played a significant role in the collapse of Alto Rio. (i) Compression damage. The bearing walls surrounding and under the staircase on gridline J between axes 26 and 28 and axes 30 and 34 at the ground floor (Level F0) were susceptible to compression damage and failure which is extremely fragile. During the forensic investigations, extensive concrete crushing was observed above and immediately below Level F0. These walls with curved corners created a complex stress state concentrating damage. The presence of a door opening at the first underground level (below Level F0) further complicated this state of stress and stress concentration, which may have reduced the overturning moment resistance and triggered the overturning collapse of the building. (ii) Yielding of the longitudinal reinforcement in tension. The contour plots of the maximum (tensile) principal strain indicate that shear walls (especially on the west side of the building) at the first two stories (F0-F2) suffered significant horizontal and diagonal tension damage. Without any special reinforcing detailing, longitudinal reinforcement that yielded in tension was prone to buckling upon crack closure. (iii) Shear damage. The analyses performed predict the formation of diagonal tension bands under and around wall openings at the first two stories (F0-F2).

The contour plots of the maximum shear strain indicate the development of large diagonal shear cracks (leading to shear failure) in transverse walls at the first two stories (F0-F2). Finally, (iv) the coupling actions between walls and slabs at each floor level, especially along the central corridor, provide additional resistance and reduce drift demands at failure, but increase the shear demand in the walls. Yielding (hinging) in the floor slabs along the central corridor has a negative impact on the structural ductility. The analyses performed also indicate that torsional effects also played a significant role in the collapse of Alto Rio. More detailed about the 3D nonlinear model of Alto Rio and the analysis results can be found elsewhere [36].

6. Acknowledgements

The China Scholarship Council (CSC) under Grant No. 201306060045 and the National Natural Science Foundation of China (NSFC) under Grant No. 51261120376 and 91315301-12 partially supported this research. Their support is gratefully acknowledged. The writers wish to thank Dr. Marios Panagiotou from Nabih Youseff & Associates and Dr. Yuan Lu from Computers & Structures, Inc. (CSI) for their technical help related to the beam-truss modeling approach. The authors are also grateful to GiD and Seismosoft for the free use of their software. Any opinions, findings, conclusions or recommendations expressed in this publication are those of the writers and do not necessarily reflect the views of the sponsoring agencies.

7. References

[1] R. Boroschek, P. Bonelli, J.I. Restrepo, R. Retamales, and V. Contreras. (2014). "Lessons from the 2010 Chile Earthquake for performance based design and code development." Journal of Symbolic Logic, 11(3), 75-79.

[2] O. Mahul and E. White. (2012). Knowledge Note 6-2 Cluster 6: The economics of disaster risk, risk management, and risk financing. Earthquake Risk Insurance, World Bank, Washington D C.

[3] IDIEM. (2010). Peritaje Estructural Edificio Alto Río Ciudad de Concepción, Prospección y Ensayo de Materiales. Informe Final No. 644.424-07, Santiago, Chile.

[4] IDIEM. (2010). Peritaje Estructural Edificio Alto Río Ciudad de Concepción-Descripción de Caída y Factores Asociados al Colapso. Informe Final No. 644.424-00, Revisión 1, Santiago, Chile.

[5] DICTUC. (2010). Propiedades Mecánicas de los Materiales: Extracción y Ensayo de Testigos, Contrastación Geométrica Parcial Condominio Alto Río – Edificio Torre Padre Hurtado – Concepción. Informe 885880, Santiago, Chile.

[6] A. Alimoradi and F. Naeim. (2010). "Did the large coseismic displacement cause the global overturning collapse of the Alto Rio building during the 27 February 2010 offshore Maule, Chile Earthquake?" The Structural Design of Tall and Special Buildings, 19(8SI), 876-884.

[7] C. Song, S. Pujol, and A. Lepage. (2012). "The collapse of the Alto Río building during the 27 February 2010 Maule, Chile, Earthquake." Earthquake Spectra, 28(S1), S301-S334.

[8] M. Kohrangi. (2012). "Seismic assessment of a 15-story building damaged in the Chile earthquake of February 27th 2010." 15th World Conference in Earthquake Engineering, Lisbon, Portugal.

[9] American Society of Civil Engineers (ASCE). (2000). Prestandard and commentary for the seismic rehabilitation of buildings. FEMA 356, Federal Emergency Management Agency, Washington, D.C.

[10] Z.T. Değer and J.W. Wallace. (2015). Collapse assessment of the Alto Rio building in the 2010 Chile Earthquake. Earthquake Spectra, 31(3), 1397-1425.

[11] National Institute of Standards and Technology (NIST). (2014). Recommendations for seismic design of reinforced concrete wall buildings based on studies of the 2010 Maule, Chile Earthquake, GCR 14-917-25.

[12] J.I. Restrepo, J.P. Conte, R.S. Dunham, D. Parker, J. Wiesner, and P. Dechent. (2016). "Detailed nonlinear FE pushover analysis of Alto Rio Building." 16th World Conference in Earthquake Engineering, Santiago, Chile.

[13] F. Mckenna, G.L. Fenves, M.H. Scott, and B. Jeremic. (2000). Open system for earthquake engineering simulation. PEER, University of California, Berkeley, Available from URL: http://opensees.berkeley.edu.

[14] Retrieved from SkyscraperPage.com: http://skyscraperpage.com/cities/?buildingID=85186.

[15] F. James. (2010). Collapsed Chile apartment tower yields 25 survivors: AP. Retrieved from NPR website: http://www.npr.org/blogs/thetwo-way/2010/03/collapsed_chile_apartment_towe.html.

[16] INN. (2008). NCh 430.Of 2008, Hormigón armado – Requisitos de diseño y cálculo, Santiago, Chile.

[17] F. Rojas, M. Lew, and F. Naeim. (2010). "An overview of building codes and standards in Chile at the time of the 27 February 2010 offshore Maule, Chile Earthquake." The Structural Design of Tall and Special Buildings, 19(8), 853-865.

[18] ACI 318-05. (2005). Building code requirements for structural concrete and commentary. American Concrete Institute (ACI) Committee 318, Farmington Hills, Michigan.

[19] Nevada Geodetic Laboratory. Available from URL: http://geodesy.unr.edu/NGLStationPages/stations/CONZ.sta.

[20] S. Banville and R.B. Langley. (2010). "Instantaneous cycle-slip correction for real-time PPP applications." Navigation - Journal of The Institute of Navigation, 57(4), 325-334.

[21] C. Vigny, A. Socquet, S. Peyrat, J.-C. Ruegg, M. Métois, R. Madariaga, S. Morvan, M. Lancieri, R. Lacassin, J. Campos, et al. (2011). "The 2010 Mw 8.8 Maule megathrust earthquake of Central Chile, monitored by GPS. Science, 332(6036), 1417-1421.

[22] S. Midorikawa, H. Yamanaka, K. Chimoto, R. Riddell, H. Miura, and K. Saguchi. (2014). "Evaluation of site effects on strong-motion records in Concepción during the 2010 Maule, Chile, Earthquake." Bulletin of the Seismological Society of America, 104(5), 2503-11.

[23] G.A. Montalva, F.J. Chávez-Garcia, A. Tassara, D.M.J. Weisser. (2015). "Site effects and building damage characterization in Concepción after the Mw 8.8 Maule Earthquake." Earthquake Spectra, 32(3), 1469-1488.

[24] Y. Lu and M. Panagiotou. (2014). "Three-dimensional cyclic beam-truss model for nonplanar reinforced concrete walls." Journal of Structural Engineering, ASCE, 140(3), 328-329.

[25] M. Panagiotou, J.I. Restrepo, M. Schoettler, and K. Geonwoo. (2012). "Nonlinear cyclic truss model for reinforced concrete walls." Structural Journal, ACI, 109(2), 205-214.

[26] Y. Lu, M. Panagiotou, and I. Koutromanos. (2014). Three-dimensional beam-truss model for reinforced concrete walls and slabs subjected to cyclic static or dynamic loading. PEER Report 2014/18, Pacific Earthquake Engineering Research Center, University of California, Berkeley.

[27] F.J. Vecchio and M.P. Collins. (1986). "The modified compression field theory for reinforced concrete elements subjected to shear." Structural Journal, ACI, 83(2), 219-231.

[28] R. Park, M.J.N. Priestley, and W.D. Gill. (1982). "Ductility of square-confined concrete columns." Journal of the Structural Division, ASCE, 108(4), 929-950.

[29] Z.P. Bažant and J. Planas. (1998). Fracture and size effect in concrete and other quasibrittle materials, CRC Press, Boca Raton, Florida.

[30] F. Filippou, E. Popov, and V. Bertero. (1983). Effects of bond deterioration on hysteretic behavior of reinforced concrete joints. Report No. UCB/EERC-83/19, University of California, Berkeley.

[31] Matlab. (2012). The MathWorks Inc., Natick, Massachusetts, US. Available from URL: http://cn.mathworks.com.

[32] GiD. (2016). The personal pre and post processor. Available from URL: www.gidhome.com.

[33] Instituto de Investigación Tecnológica. (2012). Revisión Estructural Proyecto: "Condominio Alto Río. Edificio Padre Hurtado". Concepción, Universidad de Concepción.

[34] M. Panagiotou and J.I. Restrepo. (2011). Computational models for the UCSD 7-story structural wall building slice, Report No. SSRP–07/09, Department of Structural Engineering, University of California, San Diego.

[35] M. Panagiotou and J.I. Restrepo. (2011). "A displacement-based method of analysis for regular reinforced concrete wall buildings: Application to a full-scale 7-story building slice tested at UC San Diego." Journal of Structural Engineering, ASCE, 137(6), 677-690.

[36] P. Zhang, J.I. Restrepo, J.P. Conte, and J. Ou. (2016). "Nonlinear finite element modeling and response analysis of the collapsed Alto Rio building in the 2010 Chile Maule Earthquake." The Structural Design of Tall and Special Buildings, under review.